AIAA-2003-4000

A GENERALIZED MULTI-PHASE FRAMEWORK FOR MODELING CAVITATION IN CRYOGENIC FLUIDS

A. Hosangadi and V. Ahuja

Combustion Research and Flow Technology, Inc. (CRAFT Tech)
Dublin, PA 18917

33rd AIAA Fluid Dynamics Conference
23-26 June, 2003 / Orlando, FL

A GENERALIZED MULTI-PHASE FRAMEWORK FOR MODELING CAVITATION IN CRYOGENIC FLUIDS

Ashvin Hosangadi[†] and Vineet Ahuja[††]
Combustion Research and Flow Technology, Inc.
Dublin, PA 18917
hosangad@craft-tech.com

Abstract

A generalized multi-phase formulation for cavitation in fluids operating at temperatures elevated relative to their critical temperatures is presented. The thermal effects and the accompanying property variations due to phase change are modeled rigorously. Thermal equilibrium is assumed and fluid thermodynamic properties are specified along the saturation line using the NIST-12 databank. Fundamental changes in the physical characteristics of the cavity when thermal effects become pronounced are identified; the cavity becomes more porous, the interface less distinct, and has increased entrainment when temperature variations are present. Quantitative estimates of temperature and pressure depressions in both liquid nitrogen and liquid hydrogen were computed and compared with experimental data of Hord [1] for hydrofoils. Excellent estimates of the leading edge temperature and pressure depression were obtained while the comparisons in the cavity closure region were reasonable. Liquid nitrogen cavities were consistently found to be in thermal equilibrium while liquid hydrogen cavities exhibited small, but distinct, non-equilibrium effects.

1.0 Introduction

Our focus is on the development of a computational framework to simulate cavitating liquid rocket turbomachinery. Liquid rocket systems are a subset of a broader class of pumps (e.g. refrigerant systems, boiler feed pumps, etc) where the operating temperature is elevated relative to the critical temperature of the fluid and thermodynamic effects of cavitation play an important role. At these operating temperatures, the ratio of liquid to vapor density is lower and consequently more liquid mass has to vaporize to sustain a cavity. Therefore evaporative cooling effects are more pronounced and result in the lowering of the mean fluid temperature in the cavitating region. Since the fluid thermodynamics properties (i.e. vapor pressure, density) are a strong function of temperature at these conditions, thermal effects suppress cavitation and lower the cavity pressure in a mean sense. Typically this results in improved mean performance of cryogenic pumps; liquid hydrogen systems being an extreme example where the pump may continue to generate head even when the fluid is boiling at the inlet.

The thermal effects of cavitation were studied extensively by numerous researchers through the 1970's including: Stahl and Stepanoff [2], Ruggeri and Moore [3], Hord [1], Holl et al. [4], and Brennen [5] among others. Stahl and Stepanoff [2] were the first to estimate head depression (ΔH_v) values due to thermodynamic effects using the so-called 'B-factor' method based on a quasi-static theory where the temperature depression was estimated in terms of the ratio of the vapor volume to liquid volume. They provided a graph to evaluate NPSH corrections for hydrocarbons based on this methodology. More elaborate correlations, which included dynamic effects were given later by Ruggeri and Moore [3], Hord [1], and Holl [4]. They collected extensive experimental data of cavity pressure and temperature depressions for a variety of model shapes and fluids and correlated the results using variants of the B-factor theory. The semi-empirical procedures outlined by Ruggeri and Moore [3] continues to be used as an engineering tool for predicting the predicting the thermodynamic depression in pumps. A more rigorous numerical procedure was developed by Cooper [6] where a baratropic equation of state was used to define the two-phase mixture and thermal effects were evaluated with a resulting non-dimensional vaporization parameter. Most of these techniques, however, require some degree of empiricism. Therefore, from a more fundamental modeling perspective, this discussion highlights the need for a generalized compressible formulation that takes the energy balance into account when simulating cavitation for cryogenic flows.

The development of numerical models to simulate cavitating flows has continued to receive attention from a broad range of research groups.

*AIAA-2003-4000, 33rd AIAA Fluid Dynamics Conference, Orlando, FL, June 23-26, 2003.

[†] Principal Scientist, Member AIAA

[††] Research Scientist, Member AIAA

However, the vast majority of these efforts have not considered the more general case of cavitation with thermal effects and variable fluid properties. For the purposes of our discussion here, Cavitation models in CFD tools may broadly be classified into two categories: a) A bubbly framework using the Rayleigh-Plesset equation, and b) Continuum formulation solving for gas phase transport. We note in this section, no distinction is made between non-condensable gas and vapor when referring to "gas" volume and mass fractions. There have been numerous numerical studies using the bubbly closure model (e.g., Kubota et al. [7], Colonius et al., [8]). Here, the flowfield is seeded with bubbles and the change in bubble mass (and therefore the mixture density in each cell) is obtained from the Rayleigh-Plesset equations. The advantage of this formulation is that a physical model describes the cavitation phase change. However, the *key limitation* of these studies arises from their implicit restriction that the mixture be "dilute" i.e., the gas void fraction be negligibly small. For instance, Kubota et al., [7] define mixture density as $\rho_m = (1-\phi_g)\rho_l$ which neglects the vapor phase. When $\phi_g \approx 1$ the conservation equations for the mixture become singular. This is a severe restriction. In particular, for cloud cavitation problems where the vapor clouds are very dense and the spatial extent of each distinct cloud can be large, the flowfield within the gas phase has to be resolved numerically.

The second approach followed is a continuum formulation that is applicable to dense cavitating flow (e.g. Venkateswaran et al. [9], Singhal [10], Ahuja et al. [11][12], and Senocak and Shyy [13]). Here, a separate equation for the transport of the gas phase is solved for and there is no restriction on the volume fraction of the gas-phase being small. The cavitation process is modeled as a phase change source term. Cavitation is typically modeled with a rate equation for phase change based on the local pressure. While the works referenced above use different formulations to specify this rate of phase change, they are similar in that they do not integrate the cloud bubble dynamics since neither the radius nor the number density of the bubbles in the vapor cloud are computed. In general, good results are obtained for the mean cavitation solutions. We note that this is also the cavitation phase change model used in the present study. However, for unsteady cloud cavitation, the development of more rigorous unsteady cavitation models will be necessary.

For turbomachinery simulations, CFD technology is currently limited to simulating mean cavitating performance *at design* conditions for idealized liquids (no thermodynamic effects). Typical simulations show comparisons with data at design conditions for the head coefficient and the critical Nss number at which performance breakdown occurs (Hosangadi et al. [14], Athavale and Singhal, [15], Dupont and Okamura [16], Medvitz et al., [17]). However flows at off-design conditions, where large scale unsteadiness and high dynamic pressure loads are observed, cannot at this point be reliably predicted Simulation of cavitation instabilities and rotational cavitation modes in pumps have not been simulated by any group to the best of our knowledge. Thus, to develop a CFD simulation framework that can eventually simulate unsteady, off-design performance of liquid rocket turbopumps, significant development will be required from the current level of technology.

The focus of this paper is on the development of a generalized framework that can model cavitation in liquid with variable properties and rigorously account for the thermal effects of cavitation. This framework will be the foundation for the eventual goal of our effort to model unsteady performance of liquid rocket pumps. With this is mind, the equations are cast in an acoustically accurate form and is an extension of earlier work by the authors for idealized liquids (Ahuja et al. [12]). The rigorous acoustic treatment of the gas/liquid interface captures the coupling of the phase change process with the dynamic pressure field which is an important attribute for unsteady cloud cavitation problems where high amplitude, localized pressure spikes can occur (Hosangadi et al. [18]).

The numerical code utilized in our simulations is the CRUNCH CFD® code, which is a multi-element based unstructured code [19],[20]. The underlying philosophy in the CRUNCH CFD® code is to tailor the grid topology to resolving the dominant flow phenomena and the structural complexity of the problem. This is achieved by utilizing a combination of hexahedral, tetrahedral, prismatic and pyramidal elements in mesh construction. Such a framework is particularly attractive for complex turbomachine configurations, since high quality grids can be generated very efficiently with minimum skewness.

Rigorous validation for cavitation in both liquid nitrogen and hydrogen is provided by simulating experimental measurements of Hord [1]. Detailed comparisons of pressure and temperature depressions in the cavity are presented. We also provide a discussion of how variable fluid properties and thermal effects alter the physical characteristics of the cavity. These changes such as frothy cavitation zones and increased entrainment in cavities have been observed experimentally and we use the numerical framework to identify the physics driving these effects. Furthermore, we examine some of the

assumptions of the B-factor theory as well as the applicability of thermal equilibrium criteria for cavitation in cryogenic fluids. Since the cavitation process couples strongly with the temperature of the liquid, cavitation in cryogenic system presents a far richer spectrum of physics. For instance, cavity length depends not just on the freestream pressure (or cavitation number) but also on the freestream velocity with temperature depression values being a function of the dynamic head. Here we present parametric studies for a range of freestream temperatures and velocities to identify many of the characteristics of cavitation in cryogenic fluids.

2.0 Multi-Phase Equation System

The multiphase equation system is written in vector form as:

$$\frac{\partial Q}{\partial t}+\frac{\partial E}{\partial x}+\frac{\partial F}{\partial y}+\frac{\partial G}{\partial z}=S+D_v \qquad (1)$$

Here Q is the vector of dependent variables, E, F and G are the flux vectors, S the source terms and D_v represents the viscous fluxes. The viscous fluxes are given by the standard full compressible form of Navier Stokes equations (Hosangadi [19]). The vectors Q, E and S are given below with a detailed discussion on the details of the cavitation source terms to follow later:

$$Q=\begin{pmatrix}\rho_m\\ \rho_m u\\ \rho_m v\\ \rho_m w\\ \rho_g\phi_g\\ \rho_m h_m\\ \rho_m k\\ \rho_m \varepsilon\end{pmatrix} \quad E=\begin{pmatrix}\rho_m u\\ \rho_m u^2+P\\ \rho_m uv\\ \rho_m uw\\ \rho_g\phi_g u\\ \rho_m h_m u\\ \rho_m ku\\ \rho_m \varepsilon u\end{pmatrix} \quad S=\begin{pmatrix}0\\ 0\\ 0\\ 0\\ S_g\\ S_h\\ S_k\\ S_\varepsilon\end{pmatrix} \qquad (2)$$

Here, ρ_m and h_m are the mixture density and enthalpy respectively, and ϕ_g is the volume fraction or porosity of the vapor phase. The mixture energy equation has been formulated with the assumption that the contribution of the pressure work on the mixture energy is negligible which is a reasonable assumption for this flow regime. The source term for the vapor phase arises from rate of vapor mass generation due to cavitation m_t and the corresponding source term for the energy equation is given as $m_t \cdot h_{fg}$ where h_{fg} is the change in enthalpy resulting from the phase change and is a function of the local fluid temperature.

The mixture density and gas porosity are related by the following relations locally in a given cell volume:

$$\rho_m = \rho_g \phi_g + \rho_L \phi_L \qquad (3)$$

$$1 = \phi_g + \phi_L \qquad (4)$$

where ρ_g, ρ_L are the physical material densities of the gas and liquid phase respectively and in general are functions of both the local temperature and pressure.

Thus far we have not made any statements defining the temperatures characterizing the liquid and vapor. In general, the liquid and vapor may not be in equilibrium locally and can have independent temperatures. Examination of temperature and pressure data for cavitation in Freon by Ruggeri [21] (see Figure 1) reveals that the saturation vapor pressure corresponding to the local fluid temperature in fact matches the local pressure measurement. This indicates local thermodynamic equilibrium that is exploited to significantly simplify Eqn. (1). The thermodynamic properties of the liquid and vapor in the cavity may now be defined by a single variable; the saturation temperature T_{sat}. Hence, all thermodynamic properties (density, vapor pressure, viscosity, etc) of both the liquid and the vapor phase may be generated as a tabular function of the saturation temperature. In our study here, these properties were generated from the Standard thermodynamic database 12 available from NIST for pure fluids.

The equation system as formulated in Eqn. (1) is very stiff since the variations in density are much smaller than the corresponding changes in pressure. Therefore to devise an efficient numerical procedure we wish to transform Eqn. (1) to a pressure based form where pressure rather than density is the variable solved for. An acoustically accurate two-phase form of Eqn. (1) is first derived, followed by a second step of time-scaling or preconditioning to obtain a well-conditioned system. We begin by defining the acoustic form of density differential for the individual gas and liquid phase as follows:

$$d\rho_g = \frac{1}{c_g^2}dP, \quad d\rho_l = \frac{1}{c_L^2}dP \qquad (5)$$

Here c_g is the isothermal speed of sound $\left(\frac{\partial P}{\partial \rho_g}\right)_T$ in the pure gas phase, and c_L is the corresponding isothermal speed of sound in the liquid

phase, which is a finite-value. We note that in Eqn. (5) the variation of the density with temperature has been neglected in the differential form. This assumption was motivated by the fact that the temperature changes are primarily due to the source term and not by the pressure work on the fluid i.e. the energy equation is a scalar equation. This simplifies the matrix algebra for the upwind flux formulation significantly, at the potential expense of numerical stability in a time-marching procedure. However, more importantly, there is no impact on the accuracy since the fluid properties themselves are taken directly from the thermodynamic data bank for each fluid.

Following the discussion above, the differential form of the mixture density ρ_m using Eqn. (5) is written as,

$$d\rho_m = (\rho_g - \rho_L)\,d\phi_g + \frac{1}{c_\phi^{\,2}}\,dP \qquad \left(\frac{1}{c_\phi^{\,2}} = \frac{\phi_g}{c_g^{\,2}} + \frac{\phi_L}{c_L^{\,2}}\right) \tag{6}$$

Here, c_ϕ is a variable defined for convenience and is not the acoustic speed, c_m, in the mixture, which will be defined later. Using Eqn. (6), Eqn. (1) may be rewritten as:

$$\Gamma\frac{\partial Q_v}{\partial t} + \frac{\partial E}{\partial x} + \frac{\partial F}{\partial y} + \frac{\partial G}{\partial z} = S + D_v \tag{7}$$

and,

$$Q_V = \left[p, u, v, w, \phi_g, k, \varepsilon\right]^T \tag{8}$$

The numerical characteristics of the Eqn. (7) are studied by obtaining the eigenvalues of the matrix, $\left[\Gamma^{-1}\left(\frac{\partial E}{\partial Q_v}\right)\right]$. The eigenvalues of the system are derived to be:

$$\Lambda = \left(u + c_m,\ u - c_m,\ u, u, u, u, u\right) \tag{9}$$

where c_m turns out to be the well-known, harmonic expression for the speed of sound in a two-phase mixture and is given as:

$$\frac{1}{c_m^{\,2}} = \rho_m\left[\frac{\phi_g}{\rho_g c_g^{\,2}} + \frac{\phi_L}{\rho_L c_L^{\,2}}\right] \tag{10}$$

The behavior of the two-phase speed of sound is plotted in Figure 2 as a function of the gas porosity; at either limit the pure single-phase acoustic speed is recovered. However, away from the single-phase limits, the acoustic speed rapidly drops below either limit value and remains at the low-level in most of the mixture regime. As a consequence, the local Mach number in the interface region can be large even in low speed flows.

To obtain an efficient time-marching numerical scheme, preconditioning is now applied to the system in Eqn. (7), in order to rescale the eigenvalues of the system so that the acoustic speeds are of the same order of magnitude as the local convective velocities

3.0 Cavitation Source Terms

In the present effort, the cavitation source term is defined via a simplified non-equilibrium, finite rate form as follows:

$$m_t = K_f \rho_L \phi_L + K_b \rho_g \phi_g \tag{11}$$

where the constant K_f is the rate constant for vapor being generated from liquid in a region where the local pressure is less than the vapor pressure. Conversely, K_b is the rate constant for reconversion of vapor back to liquid in regions where the pressure exceeds the vapor pressure. Here, the rate constants are specified using the form given by Merkle et al. [22].

$$K_b = \begin{bmatrix} 0 & p < p_v \\ \frac{1}{\tau_b}\left(\frac{Q_\infty}{L_\infty}\right) & \left[\frac{p - p_v}{\frac{1}{2}\rho_\infty Q_\infty^{\,2}}\right] \quad p > p_v \end{bmatrix}$$

$$K_f = \begin{bmatrix} 0 & p > p_v \\ \frac{1}{\tau_f}\left(\frac{Q_\infty}{L_\infty}\right) & \left[\frac{p - p_v}{\frac{1}{2}\rho_\infty Q_\infty^{\,2}}\right] \quad p < p_v \end{bmatrix} \tag{12}$$

$$p_v = p_\infty - \frac{1}{2}\rho_\infty Q_\infty^{\,2} * Cav.No.$$

τ_f = Time constant for vapor formation

τ_b = Time constant for liquid reconversion

$$Cav.\ No. = \frac{p_\infty - p_v}{\frac{1}{2}\rho_\infty Q_\infty^{\,2}}$$

We note that for steady attached cavitation this simplified form may be adequate since the cavitation time scales do not interact with the fluid time scales if the cavitation rate constants are fast enough. For unsteady cavitation modeling, however, it becomes

essential to integrate bubble dynamics within a dense cloud framework wherein both the number density and mean local radius of the bubbles in an evolving cloud are tracked. The development of a more rigorous non-equilibrium source term model is a topic of ongoing research.

4.0 Cavitation In Cryogenic Fluids

Detailed simulations of cavitation in liquid nitrogen and liquid hydrogen for flow over two-dimensional bodies have been conducted. We begin with a discussion of the effects of thermal effects and fluid property variation on the physical characteristics of cavitation. Quantitative estimates of pressure and temperature depression in both liquid nitrogen and hydrogen are provided by simulating experiments of Hord [1] on a hydrofoil. Effects of freestream temperature as well as velocity on the leading edge pressure and temperature depression are evaluated by conducting parametric studies. The validity of the thermal equilibrium assumption is carefully evaluated for both liquid nitrogen and hydrogen.

4.1 Impact of Temperature Variations on Cavity Characteristics

To understand the impact of temperature effects on cavitation we simulate liquid nitrogen at a temperature of 89 K, and a velocity of 20 m/s flowing over a headform of 1 inch diameter. The freestream pressure of the liquid nitrogen is 360 KPa, which corresponds to a freestream cavitation number of 0.2.

The effect of evaporative cooling at these conditions is deduced by artificially altering the heat of vaporization for liquid nitrogen while keeping all other thermodynamic properties identical to that provided by the NIST databank.

Fig. 3 shows the vapor volume fraction in the cavity for the following three different heat of vaporization factors: 1) Isothermal, $h_{vap} = 0.0$, 2) $h_{vap} = 0.1 * h_{fg}$, 3) $h_{vap} = h_{fg}$. There is a distinct change in the character of the cavity as thermal effects become more pronounced. For the isothermal case, a sharp and distinct cavity is obtained with vapor volume fraction in the cavity being near unity. As the thermal effects become pronounced the cavity interface becomes less sharp and the volume fraction of vapor in the cavity drops dramatically; for the correct heat of vaporization, the volume fraction at the leading edge is approximately 0.5 with the volume fraction in the interior being even smaller. The cavity shape also changes substantially due to the variation in physical properties: the cavity length becomes smaller while the interface itself spreads out more causing larger entrainment of liquid. Both these effects have been observed experimentally. Sarosdy and Acosta, [23] compared cavitation in water and Freon for identical B-Factors and noted that the cavity in Freon was "frothy" as opposed to the "glassy" cavity in water. We conjecture that the frothiness may be attributed to the lower volume fraction in the cavity that reduces the density difference. They also observed the increased spreading of the cavity Freon similar to our observations here.

The pressure profiles in the cavity are plotted in Figure 4 for the three cases discussed above. For the isothermal case, the pressure in the cavity is at a constant value given by the freestream cavitation number. With increasing thermal effects there is depression at the leading edge due to local temperature drop and a gradual relaxation back to the freestream value as the temperature rises again in the aft of the cavity as vapor condenses back to liquid. Interestingly, The effective temperature recovery and pressure rise is a lot slower in the cryogenic case compared to the isothermal case even though the rate term for phase change in the source terms had the identical value! The lower mixture density gradient in the cryogenic case results in the weakening of the reentrant jet thereby allowing the vapor phase to continue being convected downstream and provide a slower recovery. Quantitative validation of both the leading edge pressure and temperature depressions as well as the recovery of temperature and pressure in the closure region is provided in the following section.

4.2 Simulations of Cavitating Hydrofoil

We performed simulations of experiments by Hord [1] on a cavitating hydrofoil. Hord performed sub-scale tests using both liquid nitrogen and hydrogen in a blow-down tunnel. The details of the tunnel and the hydrofoil geometry are given in Figure 5. The tunnel width is 1 inch while the hydrofoil width is 0.312 inches. Hence considerable blockage effects from the tunnel wall are present and the simulation modeled the tunnel geometry. To ensure that the tunnel blockage effects were being correctly modeled we performed single-phase, non-cavitating simulations and have compared it to Hord's non-cavitating data in Figure 6. Excellent agreement is obtained giving confidence that the tunnel interaction is being captured. We note that the single-phase solution is insensitive to the Reynolds number since both liquid hydrogen and nitrogen show identical pressure profiles.

4.3 Cavitation in Liquid Nitrogen

Simulations at various freestream conditions are performed to evaluate our ability to predict the temperature and pressure depression in liquid nitrogen. The operating range of liquid nitrogen varies from roughly 70K -100K. The variation of properties along the saturation line for liquid and vapor densities as well as the vapor pressure are shown in Figure 7. At 89 K, the slope of vapor pressure curve indicates a 16 KPa increase for a 1 K change in temperature.

Four different tunnel conditions (See Table I) were simulated to discern the trends at various freestream conditions. The general characteristics of the cavitating flowfield are shown in Figure 8(a-d) for tunnel conditions in Run 290C (Table I). Figure 8a shows the temperature profile in the cavity. The strong temperature depression at the leading edge of the cavity is evident with the gradual temperature recovery due to condensation in the rear of the cavity. The vapor volume fraction is qualitatively compared with a typical flow visualization of the flow (note that the flow conditions at which this visualization was done are not reported in the Hord's report). The overall shape and features of the cavity appear to be similar. The computed pressure field indicates strong interaction between the cavity and the tunnel wall which is expected due to the relative scales of the geometry.

The quantitative comparisons of pressure and temperature depression in the cavity are compared with experimental data in Fig. 9. Note that the pressure values plotted are $(P - P_{v,\infty})$. For a non-cryogenic case this value would be zero in the cavity, while values below zero in the cryogenic case indicate pressure depression due to thermal effects. In general excellent comparison is obtained for the leading edge temperature depression of approximately 2.5 K. The temperature recovery within the cavity compares well both in their slope as well as the length of the cavity. The temperature rise in the cavity closure region shows some differences; the computed solution recovers to the freestream value more quickly than does the data, which doesn't quite fully recover to the freestream value. As per the discussion by Hord [1], this probably was due to the unsteady effects in the cavity closure region whereby the thermocouples were not always enclosed in vapor giving erroneous readings. The instrumentation error given for the chromel-gold thermocouples is 0.20 K and the computed results are within the uncertainty of the experiments.

The comparison of the pressure depression in Fig. 9 also indicates excellent overall comparison with data and within the instrumentation error bar of 0.69 N/cm^2. The leading edge pressure depression is 23.5 percent relative to the freestream vapor pressure. It further illustrates why temperature effects have a substantial impact on the performance of cryogenic pumps. The experimental data plotted includes both the actual pressure measured (symbol: circle) as well as the saturation pressure values (symbol: square) corresponding to the temperature measurements. The close match between the actual pressure and saturation pressure values indicates that the thermodynamic equilibrium assumption is valid for liquid nitrogen flows.

A parametric study of pressure and temperature depressions at three different freestream conditions is examined. In Figure 10, we compare simulations at tunnel conditions of Runs. 289C, 290C and 293A respectively in Figure 10. The three conditions are at different freestream temperatures and cavitation numbers. However, the freestream velocity is nearly identical and we can therefore compare the pressure and temperature depression trends at the same dynamic head. The comparison between the simulations and experiment, particularly the leading edge value, continue to be good over a range of cavity lengths. The thermal equilibrium assumption also continues to hold and pressure depressions in the 20 percent range are obtained at this dynamic head value.

In cryogenic (i.e. "real") fluid flow, the temperature depression due to cavitation is a function of the dynamic head and different solutions are obtained for flows at the same freestream cavitation number but different freestream velocities. In contrast, for "idealized" fluid flows, the cavitation number (or freestream pressure) is the primary flow parameter for a given set of freestream conditions. To illustrate this effect we compare simulations for Run 293A and Run294F in Fig. 11. The freestream temperature and the freestreeam pressures for the two cases are very similar but they have different velocities of 24 m/s and 9.8 m/s respectively. For the higher velocity case, the temperature depression is about 2.5 K while it is less than 1 K for the lower velocity case. The pressure depressions show the corresponding differences as well with the pressure depression relative to freestream pressure being 26 percent for the higher velocity case while only being 12 percent at the lower velocity. Thus we note that a far richer set of flow physics is associated with cavitation in cryogenic fluids governed by the coupling between energy balances and flow hydrodynamics.

4.4 Cavitation in Liquid Hydrogen

Simulations of the cavitating hydrofoil in liquid hydrogen are examined. The operational range for liquid hydrogen is between 15-25 K (see Fig. 12) and is a severe test for the numerical procedure. The slope of vapor pressure variation is higher as compared to liquid nitrogen (approximately 30 KPa/K as compared to 16 KPa/K for Liquid Nitrogen). Hence thermal effects in liquid hydrogen are even more enhanced as compared to liquid nitrogen.

Three different tunnel conditions were simulated (see Table II) with the free stream temperatures being similar (20 K) but at different freestream pressures and velocities. The comparisons of the pressure and temperature profiles are shown in Fig. 13. The leading edge temperature and pressure depressions continue to be predicted very well. Temperature profiles in the closure regions are showing larger differences but this could be due to increased unsteady effects in these flowfields.

A comparison of the pressure profiles shows excellent comparison with the saturation pressure values, which are consistent with the thermal equilibrium assumption of the numerical formulation. However, the saturation pressure levels and the actual pressure measurements show a distinct (if relatively minor) difference consistently for all the three cases simulated. This indicates that thermal equilibrium may be beginning to break down in these cases. We observe that all the liquid hydrogen runs were done at velocities greater than 50 m/s, which is roughly twice that of the liquid nitrogen runs. Given the strong dependence of the temperature depression on the dynamic head a valid question to pose is whether thermal non-equilibrium is a function of the fluid thermodynamics alone or whether it is also a function of the hydrodynamic conditions. An examination of the limited experimental data available indicates that the non-equilibrium effects were even more pronounced in cavitating liquid hydrogen venturis (Hord, [24]) where the fluid velocity was even higher at the throat section. This is an area that requires additional numerical investigation as well as additional experimental data to better characterize the non-equilibrium effects.

5.0 Summary

A generalized multi-phase formulation has been developed for cavitation in "real" fluid flows (e.g., cryogenic fluids) that operate at temperatures close to their critical temperatures. The formulation is based on a thermal equilibrium assumption between the vapor and liquid in the cavitating region. Fluid thermodynamic properties are specified along the saturation line as a function of temperature using the NIST-12 data bank. The energy equation for the mixture is solved in conjunction with the mass and momentum conservation and the evaporative cooling effects of cavitation are accounted for rigorously.

Variable fluid properties and temperature effects substantially alter the nature of the cavity. This was numerically illustrated by altering the latent heat of vaporization and by examining its effect on the cavity. As thermal effects become more pronounced, the cavity is more porous (experimentally its described as being frothy) and the interface between the vapor and liquid is less distinct. The cavity shape shows a substantial change; the cavity becomes shorter but spreads out far more.

Detailed validation has been presented to quantify temperature and pressure depression in liquid nitrogen and hydrogen by simulating the cavitating hydrofoil experiments of Hord [1]. In general excellent comparison of the leading edge pressure and temperature depression was obtained for all cases. The temperature profiles in the cavity closure show more variation and this is in part due to the unsteadiness in the data, which was not characterized. In cryogenic fluids, the freestream velocity or dynamic head is an independent parameter that determines the level of temperature and pressure depression. The lower pressure depressions and smaller cavities at lower freestream velocities but identical freestream cavitation was demonstrated.

The validity of thermal equilibrium was evaluated carefully for both liquid nitrogen and hydrogen. Thermal equilibrium appears to be valid assumption for liquid nitrogen at least over the range of velocities investigated for the hydrofoil. However for liquid hydrogen flows over the hydrofoil there was a distinct, but small, difference between the saturation pressure and physical pressure measurement indicating the possibility of non-equilibrium effects. It is unclear at this point if these non-equilibrium effects are solely a function of fluid thermodynamic properties or whether the velocity of the fluid also plays a role.

6.0 Acknowledgements

We acknowledge funding for this work through a SBIR program under Contract No.: NAS8-02098 funded by NASA Marshall Space Flight Center. The contract monitor is Dr. Dan Dorney. The technical inputs provided by Dr. Dan Dorney and Mr. Robert Garcia are gratefully acknowledged.

The authors would also like to thank Dr Paul Cooper for his help and advice in helping us better understand cavitation in cryogenic fluids. His

insights in this problem going back to his pioneering work in the 1960's were invaluable to our effort.

7.0 References

[1] Hord, J., "Cavitation in Liquid Cryogens," NASA CR-2156, January 1973.

[2] Stahl, H.A. and Stepanoff, A.J., "Thermodynamic Aspects of Cavitation in Centrifugal Pumps," *ASME J. Basic Eng.*, Vol. 78, pp. 1691-1693, 1956.

[3] Ruggeri, S.R., and Moore, R.D., "Method for Prediction of Pump Cavitation Performance for Various Liquids, Liquid Temperature, and Rotation Speeds, NASA TND-5292, 1969.

[4] Holl, J.W., Billet M.L., and Weir, D.S., "Thermodynamic Effects On Developed Cavitation," *ASME J. Fluids Eng.*, Vol. 97, No.4, pp. 507-516, 1975.

[5] Brennen, C.E., "The Dynamic Behavior and Compliance of a Stream of Cavitating Bubbles," *Journal of Fluids Engineering*, pp. 533-542, Vol. 95, 1973.

[6] Cooper, P., "Analysis of Single and Two-Phase Flows in Turbopump Inducers," *Journal of Engineering for Power*, Transactions of the ASME, pp. 577-588, 1967.

[7] Kubota, A., Kato, H. and Yamaguchi, H., "Cavity Flow Predictions Based on the Euler Equations," *J. Fluid Mech.*, Vol. 240, pp. 59-96, 1992.

[8] Colonius, T., d'Auria, F., Brennen, C.E., "Acoustic Saturation in Bubbly Cavitating Flow Adjacent to an Oscillating Wall," *Phys. Fluids*, Vol.12, No.11, pp. 2752-2761, November 2000.

[9] Venkateswaran, S., Lindau, J.W., Kunz, R.F., Merkle, C.L., "Preconditioning Algorithms For the Computation of Multi-Phase Mixture Flows," AIAA 2001-0279, 39th Aerospace Sciences Meeting & Exhibit, Reno, NV, Jan 2001.

[10] Singhal, A.K., Athavale, M-M., Li, H., and Jiang, Y., "Mathematical Basis and Validation of the Full Cavitation Model," 2001 ASME Fluids Eng Division Summer Meeting, New Orleans, LA, May 29-June 1, 2001.

[11] Ahuja, V., Hosangadi, A., Ungewitter, R. and Dash, S.M., "A Hybrid Unstructured Mesh Solver for Multi-Fluid Mixtures," AIAA-99-3330, 14th AIAA CFD Conf., Norfolk, VA, June 28-July 1, 1999.

[12] Ahuja, V., Hosangadi, A. and Arunajatesan, S., "Simulations of Cavitating Flows Using Hybrid Unstructured Meshes," *Journal of Fluids Engineering*, May/June, 2001.

[13] Senocak, I. and Shyy W., "Evaluation of Cavitation Models for Navier-Stokes Computations," *Proceedings of FEDSM'02*, 2002 ASME Fluids Engineering Division Summer Meeting, Montreal, Quebec, Canada, July 14-18, 2002.

[14] Hosangadi, A., Ahuja, V., and Ungewitter, R.J., "Simulations Of Cavitating Inducer Flowfields," 38th JANNAF Combustion Subcommittee (CS); Area: Turbomachinery for Space Launch Vehicle Propulsions Systems Session: Eglin Air Force Base, Sandestin FL, 8-12 April 2002.

[15] Athavale, M.M. and Singhal, A.K., "Numerical Analysis of Cavitating Flows in Rocket Turbopump Elements," 37th JPC, Salt Lake City, UT, July 2001.

[16] Dupont, P., and Okamura, T., "Cavitating Flow Calculations in Industry", The 9th International Symposium on Transport Phenomena and Dynamics of Rotating Turbomachinery, Honolulu, Hawaii, 2002.

[17] Medvitz, R.B., Kunz, R.F., Boger, D.A., Lindau, J.W., Yocum, A.M., Pauley, L.L., "Performance Analysis of Cavitating Flow in Centrifugal Pumps Using Multi-Phase CFD", Journal Fluids Engg., Vol. 124, pp. 377-383, 2002.

[18] Hosangadi, A., Ahuja, V., and Arunajatesan, S., "A Generalized Multi-Phase Framework for Modeling Unsteady Cavitation Dynamics and Thermal Effects, ONR Cavitation Workshop, Baltimore, MD, January 20, 2003.

[19] Hosangadi, A., Lee, R.A., York, B.J., Sinha, N., and Dash, S.M., "Upwind Unstructured Scheme for Three-Dimensional Combusting Flows," *Journal of Propulsion and Power*, Vol. 12, No. 3, pp. 494-503, May-June 1996.

[20] Hosangadi, A., Lee, R.A., Cavallo, P.A., Sinha, N., and York, B.J., "Hybrid, Viscous, Unstructured Mesh Solver for Propulsive Applications," AIAA-98-3153, AIAA 34th JPC, Cleveland, OH, July 13-15, 1998.

[21] Ruggeri, R.S., "Experimental Studies on Thermodynamic Effects of Developed Cavitation," *Proc. International Symposium on the Fluid Mechanics and Design of Turbomachinery*, Penn State University, University park, PA, Aug. – Sept. 1970.

[22] Merkle, C.L., Feng, J.Z. and Buelow, P.E.O., "Computational Modeling of the Dynamics of Sheet Cavitation," *Proceedings of the 3rd International Symposium on Cavitation*, Grenoble, 1998.

[23] Sarosdy L.R. and Acosta A.J., "Note on Observations of Cavitation in Different Fluids," Paper No. 60-WA-83, ASME Winter Annual Meeting, New York, Nov. 27- Dec. 2, 1960.

[24] Hord, J., "Cavitation in Liquid Cryogens I – Venturi," NASACR-2054, May 1972.

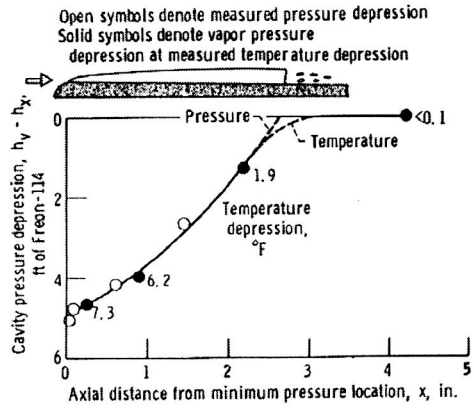

Fig. 1. Pressure Depression in Cavitation Zone for Venturi with Freon (Taken from Ruggeri, 1970).

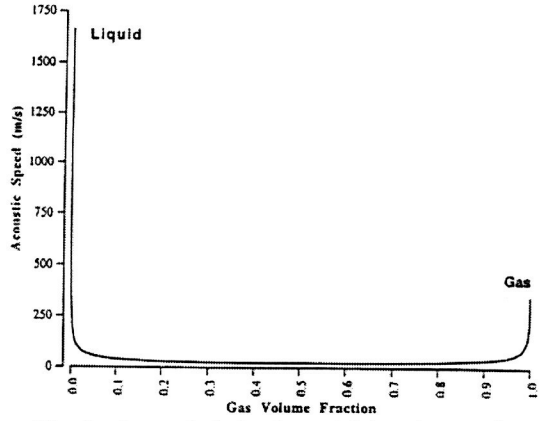

Fig. 2. Acoustic behavior exhibits a harmonic relationship with very low values in the mixture regime.

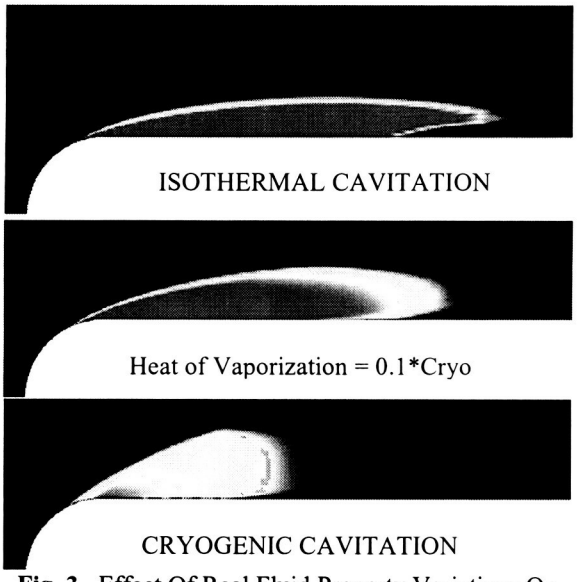

Fig. 3. Effect Of Real Fluid Property Variations On Cavity Shape and Volume Distribution.

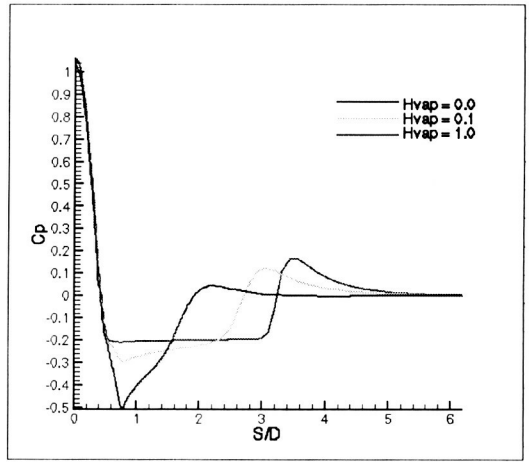

Fig. 4. Effect Of Real Fluid Property Variations On Cavity Pressure Distribution.

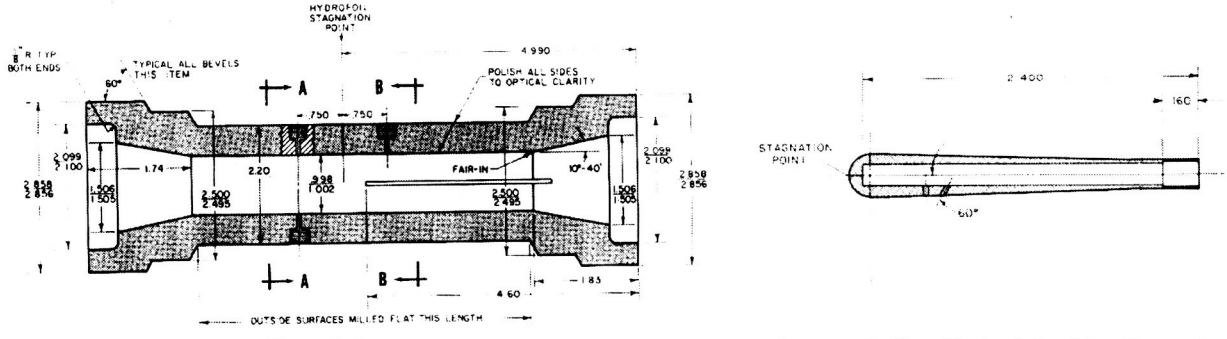

Tunnel Geometry

Quarter Caliber Hydrofoil with a Tapered Diffuser

Fig. 5. Details of Experimental Set-up for Cavitating Hydrofoil (Taken from Hord, 1973).

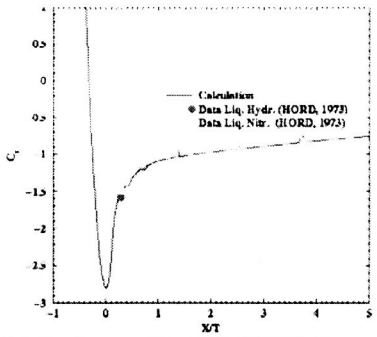

Fig. 6. Non-Cavitating Pressure Distribution on Hydrofoil With Tunnel Blockage Modeled (Hord 1973).

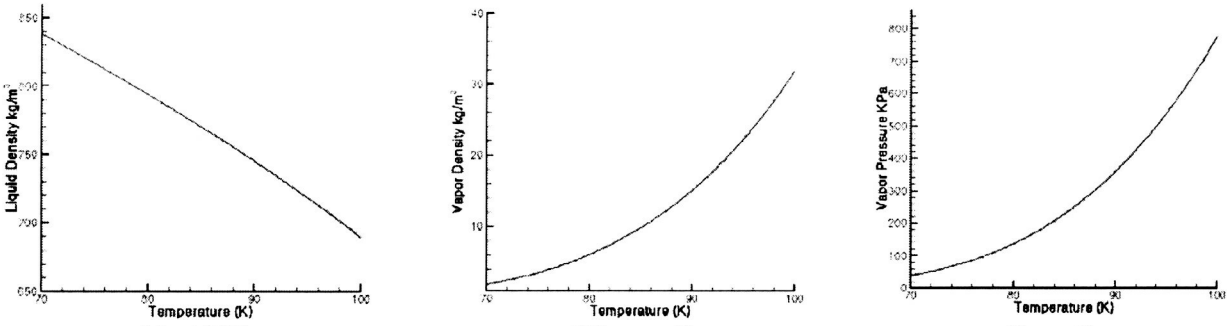

Liquid Nitrogen Nitrogen Vapor Vapor Pressure

Fig. 7. Physical Properties Of Liquid Nitrogen (Temperature Dependence).

Table I. Run Conditions For Liquid Nitrogen Cases.

RUN NUMBER	FREESTREAM TEMP. (K)	FREESTREAM VEL. (M/S)	CAVITATION NUMBER	CAVITY LENGTH (CM)
289C	88.64	23.5	1.55	2.29
290C	83.06	23.9	1.70	1.9
293A	77.64	24.0	1.75	1.52
294F	77.94	9.8	1.78	1.52

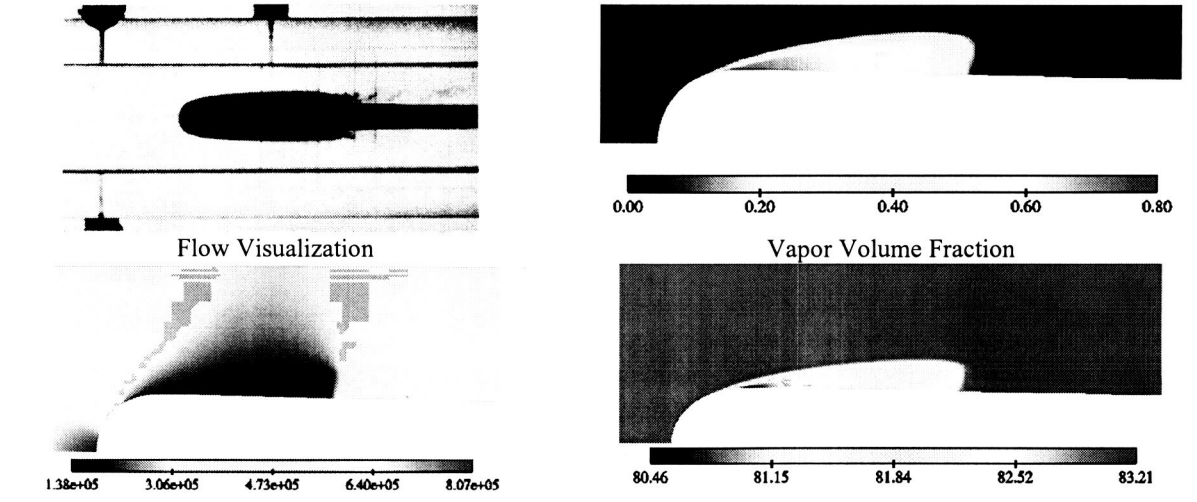

Flow Visualization Vapor Volume Fraction

Pressure Distribution Cavity Temperature

Fig. 8. Cavitating Hydrofoil Flowfield For conditions of Run 290C in Liquid Nitrogen.

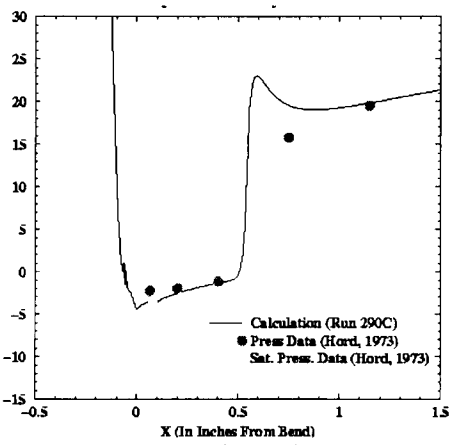

Pressure depression.

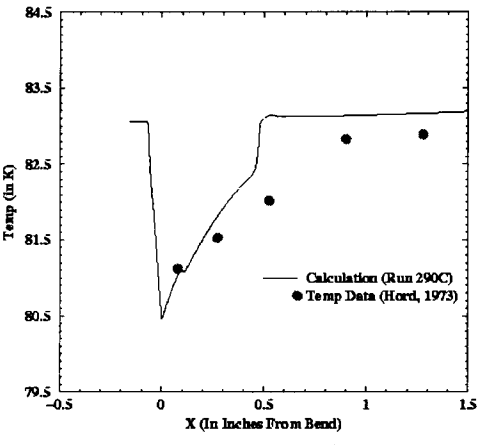

Temperature depression

Fig. 9. Comparison of Cavitating Hydrofoil Simulations with Data for Liquid Nitrogen.

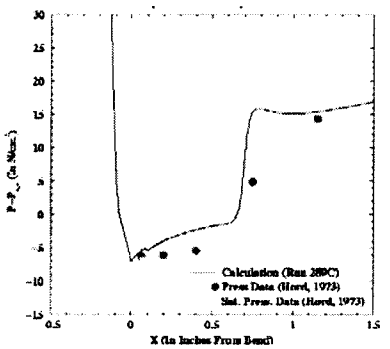

L.E. Press. Depress. = 22%

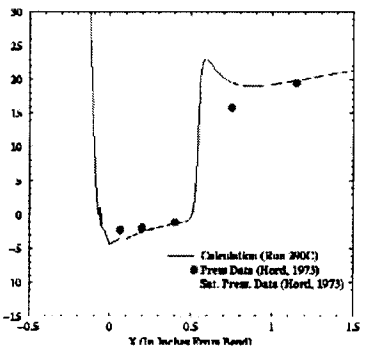

L.E. Press. Depress. = 23.5%

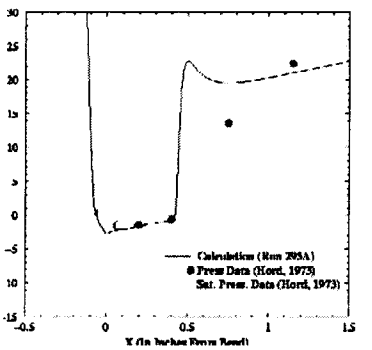

L.E. Press. Depress. = 26%

Pressure Depression

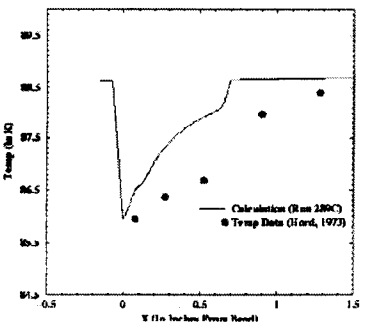

Temp= 88.64 K, Vel=23.5 m/s
Cavitation Number= 1.55
Cavity Length=0.90 in

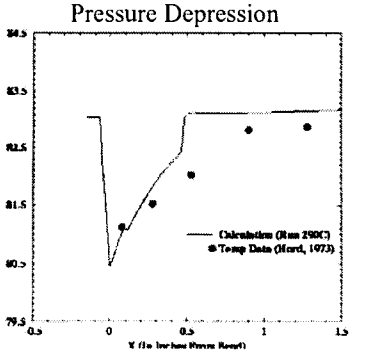

Temp= 83.64 K, Vel=23.9 m/s
Cavitation Number= 1.7
Cavity Length= 0.75 in

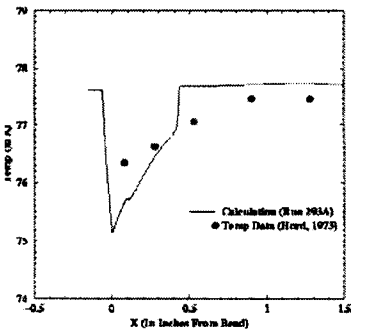

Temp= 77.64 K, Vel=24.0 m/s
Cavitation Number= 1.75
Cavity Length= 0.6 in

Temperature Depression

Fig. 10. Cavity Solutions at various Freestream Temperatures in Liquid Nitrogen.

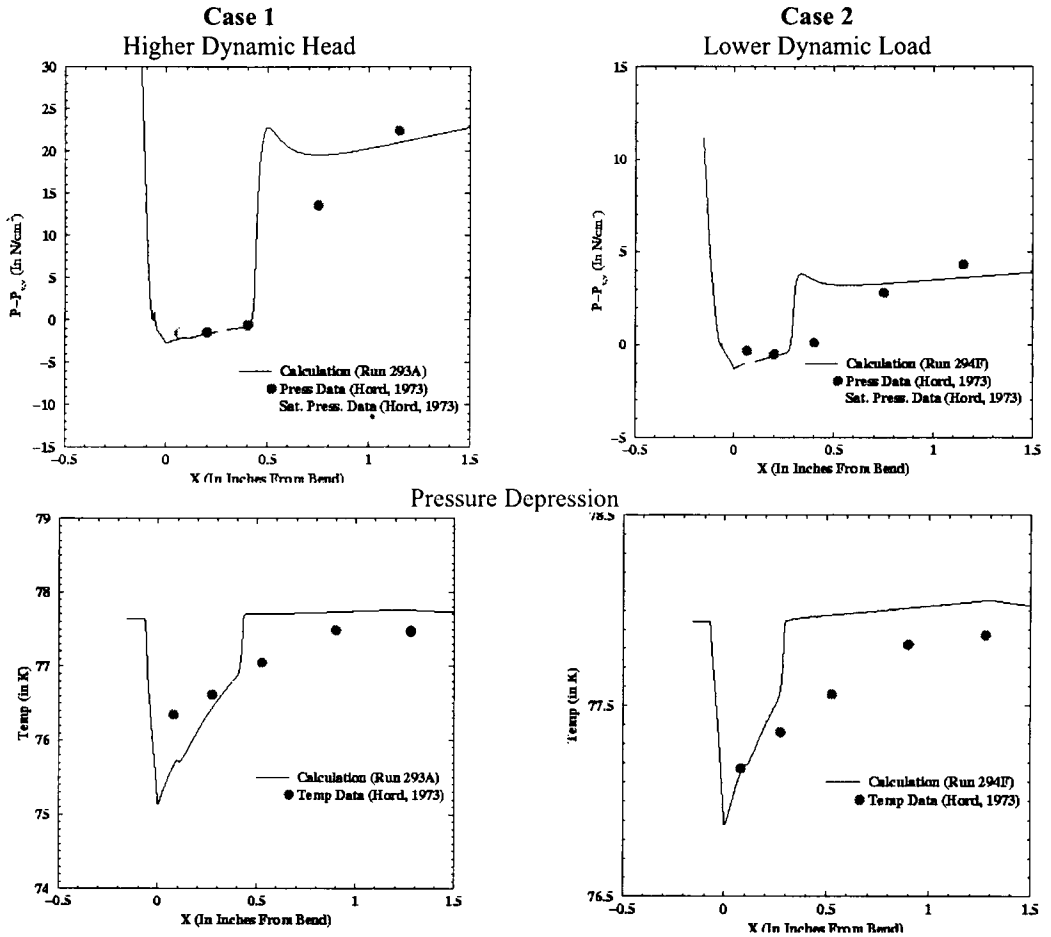

Fig. 11. Cavity Solutions at various Freestream Velocities in Liquid Nitrogen.

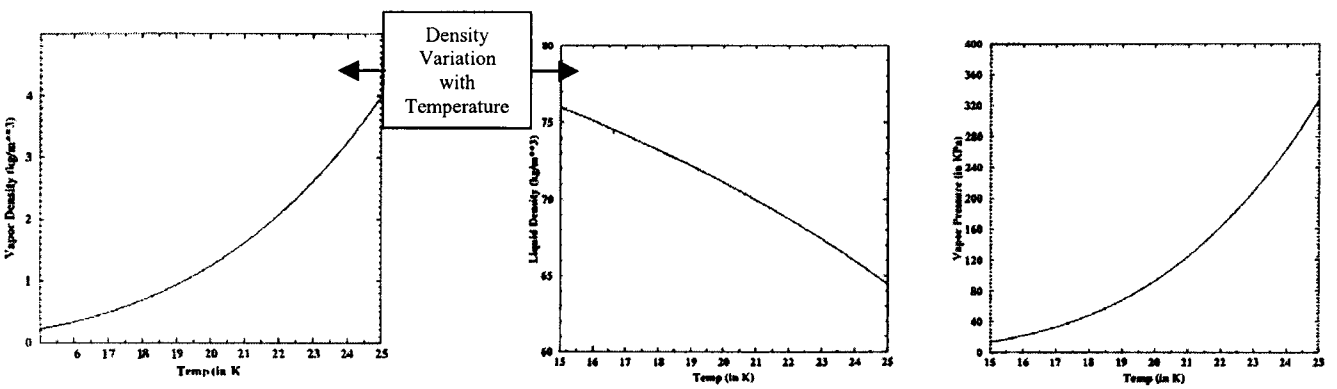

Fig. 12. Physical Properties of Hydrogen (Temperature Dependence).

Table II. Run Conditions For Liquid Hydrogen Cases.

RUN NUMBER	FREESTREAM TEMP. (K)	FREESTREAM VEL. (M/S)	CAVITATION NUMBER	CAVITY LENGTH (CM)
247B	20.69	65.2	1.68	1.52
249D	20.70	58.1	1.57	1.90
231C	20.63	51.4	1.34	1.77

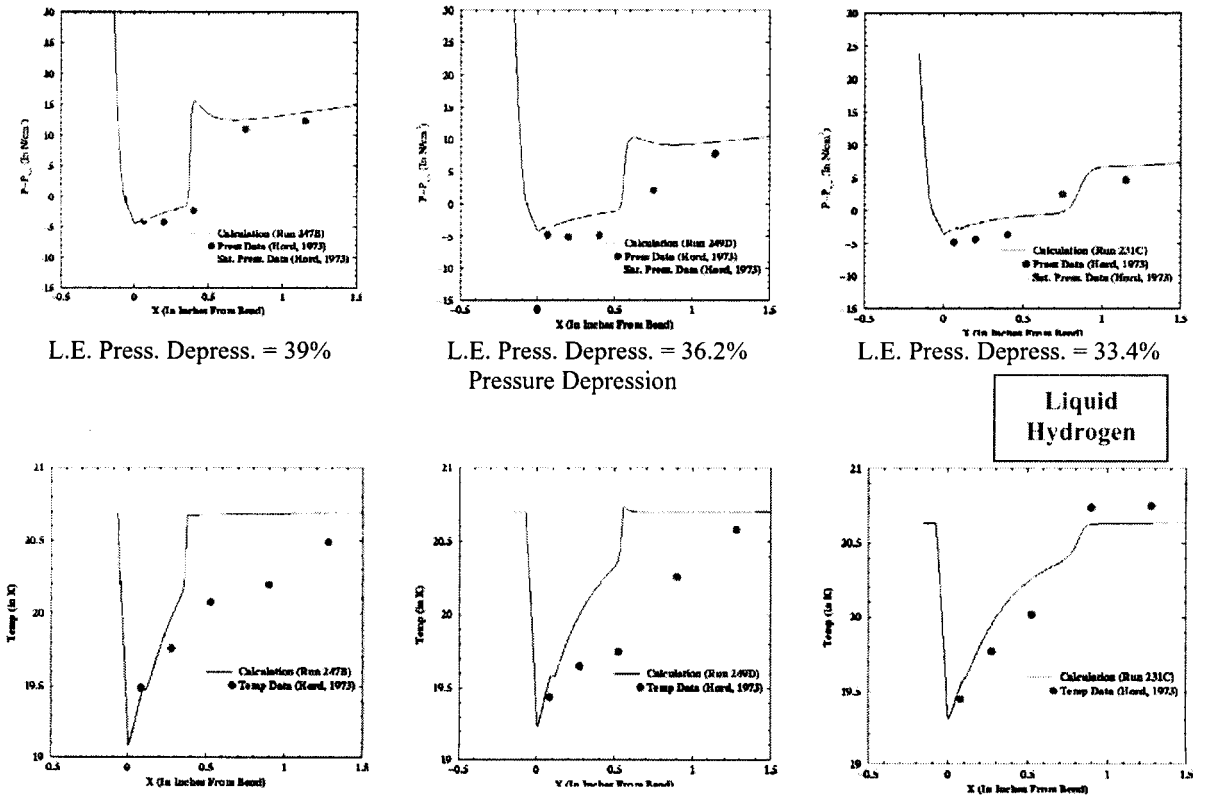

Fig. 13. Cavity Solutions at various Freestream Temperatures For Liquid Hydrogen.